COMPARISON OF SPACEBORNE AND AIRBORNE HYPERSPECTRAL IMAGING SYSTEMS FOR ENVIRONMENTAL MAPPING

Haluk Cetin

Mid-America Remote Sensing Center, Murray State University, Murray KY 42071 USA - Haluk.Cetin@MurrayState.edu

KEY WORDS: Remote Sensing, Hyperspectral, Comparison, Platforms, Land Cover Mapping, Performance, Hyperion, AVIRIS

ABSTRACT:

The main purpose of this study was to compare hyperspectral remotely sensed data collected by the Hyperion satellite, and the airborne Real-time Data Acquisition Camera System (RDACS-3) and the Airborne Visible/Infrared Imaging Spectrometer (AVIRIS) for environmental mapping and vegetation species identification. Hyperion was NASA's first hyperspectral imager aboard NASA's Earth Observing-1 (EO-1) spacecraft. The EO-1 mission had three advanced land imaging instruments; Advanced Land Imager, Hyperion, and Atmospheric Corrector. AVIRIS collects 224 contiguous spectral bands with wavelengths from 0.4 to 2.5 µm, whereas RDACS-3 has many spectral modes (64, 128, 256, etc.). The study area, Land-Between-the-Lakes (LBL), is located in western Kentucky, USA. Most of LBL consists of forested areas, which are predominantly oak and hickory, and open land areas. Twenty-five percent (17200 hectares) of LBL falls within the Biosphere Reserve. AVIRIS was flown on the Twin Otter turboprop at approximately 4000m above the ground with 4m spatial resolution on November 11, 1999 and September 10, 2001. The Hyperion provided 242 spectral bands (from 0.4 to 2.5 µm) with a 30 meter spatial resolution and covered 7.5km by 200km area on April 29, 2001. An RDACS-3 imagery with 120 spectral bands and 2x4m spatial resolution was collected at 2350m above the ground by the ITD Spectral Visions on September 7, 1999. During the overflights, ground spectra using an ASD FieldSpec-FR® spectroradiometer (0.35-2.5 µm) were collected for data calibration, spectral library construction, atmospheric correction and species identification. Moreover, multispectral satellite and aerial imagery at 1m resolution was collected for some of the test sites in the area. Several hyperspectral and multispectral processing tools were utilized for atmospheric corrections, enhancements, and classifications. Best results were obtained using the AVIRIS and RDACS-3 data. The Hyperion data also provided very good results for the mapping; however, its spatial resolution was one of the limitations of the Hyperion sensor. The statistical difference among the classifications using the sensors proved to be mostly significant.

1. INTRODUCTION

The primary goal of the NASA Earth Observation System (EOS) is to study the effects of climate on terrestrial vegetation (Huete *et al.,* 1994). The development of multispectral imaging spectrometers during the early 1970's allowed scientists for the first time to classify large areas of terrain (Marmo, 1996). This led to the advent of hyperspectral sensors with many bands and high spatial resolution, allowing for the classification of large areas with finer spectral resolution (Cloutis, 1996). Current multispectral satellites that orbit the earth have their own limitations. The multispectral satellites such as Landsat and SPOT as well as high spatial resolution sensors such as IKONOS and QuickBird have broad spectral bands. These bands cover the visible, near and middle-infrared regions of the electromagnetic spectrum (Jakubauskas and Price, 1997). This greatly reduces the ability of the multispectral sensor to spectrally discriminate between two objects on the ground (Marmo, 1996). Multispecral sensors have been utilized for many purposes including regional mapping. However,

multispectral imagery could not be used for very detailed mapping and identification of surface material, for which hyperspectral and/or ultraspectral sensors have been utilized. Unlike the multispectral classifiers, hyperspectral classifiers are used to identify objects using spectral endmembers in spectral libraries. Many attempts have been made to classify hyperspectral data using the traditional multispectral classifiers. Classification time has been very long and classification accuracy has not improved by the increased number of bands when the multi-spectral classifiers were used (Lee and Landgrebe, 1993). Another approach using hyperspectral data has been mapping of cover types based on their abundances by using spectral unmixing techniques (Adams *et al.*, 1986; Boardman 1990; Dwyer *et al.*, 1995; Mustard and Pieters, 1987).

Ecologists are now only beginning to explore the potential uses of high spatial and high spectral resolution remote sensing. For example, Schlesinger and Gramenopoulos (1996) used high spatial resolution satellite imagery and aerial photography to test for desertification in the Sahel by

examining tree densities in images collected over 51 years. In this study, no time-trend was observed, suggesting that if it is occurring at all, desertification is slower than previously thought in the Sahel. A range of ecological problems become tractable with the possibility of locating and identifying individual trees by remote sensing. At one end of the spectrum is the detection of rare individuals, genotypes, or species and at the opposite end of the spectrum is the location and identification of individual trees of a common species in a diverse community of similar species. A forester may have a particular interest in detecting the presence of rare survivors of a disease or insect pest outbreak in order to find resistant individuals. For example, many field ecologists have observed occasional large American chestnut individuals that have reached reproductive size and age despite exposure to ubiquitous chestnut blight. It may be that 99 percent of such cases can be due to chance escape from the blight, but 1 percent can be due to genetically-based resistance. Detection of a large enough sample of reproductive chestnuts to perform genetic screening could be impossible without an extensive search procedure such as that provided by remote sensing.

The identification of species resisting to different stress conditions has direct forestry and agriculture applications. The ability to identify vegetation at the species level using hyperspectral data has been difficult because of lack of information on vegetation characteristics and biochemical characterization of vegetation at canopy level (Martin and Aber, 1997).

There have been many studies comparing spaceborne and airborne multispectral imagery. However, similar comparisons could not be done for hyperspectral sensors until the successful lunch of the Hyperion sensor.

The main objective of this study was to compare hyperspectral remotely sensed data collected by the Hyperion satellite, and the airborne Real-time Data Acquisition Camera System (RDACS-3) and the Airborne Visible/Infrared Imaging Spectrometer (AVIRIS) for environmental mapping and vegetation species identification.

2. STUDY AREA

The study area is located in the Land-Between-the-Lakes (LBL) (Figure 1) National Recreation Area, which was designated in 1991 as an International Biosphere Reserve under the Man and Biosphere Programme of the United Nations Education, Scientific and Cultural Organization (UNESCO). In addition to LBL, the Reserve includes 17 surrounding counties in Kentucky and Tennessee as the area influenced economically, socially and environmentally by the management of LBL. One of the main purposes of the Biosphere Reserve Programme is to "involve industry, government, social agencies, schools, and special interest groups in management of the Reserve" and to encourage cooperation in studying and solving regional problems. The

draft Environmental Impact Statement for LBL identified more than 20,000 acres to be designated as core areas in the preferred management alternative. The remainder of the 170,000 acres of LBL serves as the buffer zone with the 17-county area is the transition zone. Many research studies concerning LBL and Kentucky Lake have been conducted at Murray State University in the last 30 years; some of which provided useful information for this research.

LBL is approximately 90 percent forested, which makes it one of the largest contiguous blocks of forested land east of the Mississippi River in the US. Ferguson Spring/Energy Lake site has been selected as a research site because of its diverse ecology including wetland and bottom land/upland forest. The dominant forest species are oak and hickory. Oak and hickory trees requiring large amounts of sunlight when they are seedlings have been the dominant overstory tree species in LBL. Forest composition of LBL would shift toward maple and beech trees, which prefer shade if it is left completely unmanaged. Maple trees do not produce nuts that wildlife can feed on maple seeds are small and winged. This would negatively impact many different wildlife species, including deer, squirrel, songbirds, and wild turkey, which for thousands of years have fed on the acorns and nuts of oak/hickory forest of LBL. Table 1 summarizes some of the overstory species found in LBL.
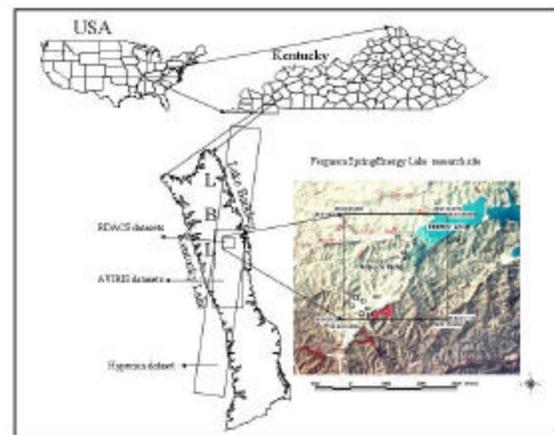

Figure 1. Location map of the study area and the datasets

The Center for Reservoir Research (CRR) was established in 1987 by the Kentucky Council on Higher Education as a Center of Excellence for Teaching and Research. CRR research has been focused mainly on Kentucky Lake water monitoring and the Kentucky Lake GIS (KLGIS). One of the principal programs of CRR is the Kentucky Lake Long Term Monitoring Program (begun in July, 1988), which encompasses 17 primary monitoring sites on the lower 30 km of the lake. The KLGIS database providing a better evaluation of the forest and wetlands in the area include bathymetry, cultural features, geology, groundwater, hydrography, soils, terrain, water quality and wetland data for the Kentucky Lake drainage basin.

Acronym	Genus	Species	Common name
POHE	Populus	heterophylla	swamp cottonwood
PRSE	Prunus	serotina	black cherry
QUAL	Quercus	alba	white oak
QUBI	Quercus	bicolor	swamp white oak
QUCO	Quercus	coccinea	scarlet oak
QUFA	Quercus	falcata	southern red oak
QUIM	Quercus	imbricaria	shingle oak
QULY	Quercus	lyrata	overcup oak
QUMA	Quercus	marilandica	blackjack oak
QUMC	Quercus	macrocarpa	bur Oak
QUMI	Quercus	michauxii	swamp chestnut oak
QUMU	Quercus	muehlenbergii	chinquapin oak
QUNI	Quercus	nigra	water oak
QUPA	Quercus	pagoda	cherrybark oak
QUPH	Quercus	phellos	willow oak
QUPL	Quercus	palustris	pin oak
QUPR	Quercus	prinus	chestnut oak
QURU	Quercus	rubra	northern red oak
QUSH	Quercus	shumardii	shumard oak
QUST	Quercus	stellata	post oak
QUVE	Quercus	velutina	black oak
RHCA	Rhamnus	caroliniana	carolina buckthorn
ROPS	Robinia	psuedoacacia	black locust
SAAL	Sassafras	albidum	sassafras
SANI	Salix	nigra	black willow
TADI	Taxodium	distichum	bald cypress
ULAL	Ulmus	alata	winged elm
ULAM	Ulmus	americana	american elm
ULRU	Ulmus	rubra	slippery elm

Table 1. Summary of tree species found in LBL.

High spectral resolution (ultraspectral) leaf, soil, and water reflectance data were collected on a regular basis with an ASD Field Spec FR®, a full-range field spectroradiometer, in the field to create a spectral library to aid the classification of the surface material. During the satellite and aerial data collection events, ground spectra were also collected for selected spectral targets.

3. IMAGERY

Several hyperspectral remotely sensed datasets collected by the Hyperion satellite (Figure 2) on April 29, 2001, and the airborne RDACS-3 (Figure 3) on on September 7, 1999 were utilized in this research. AVIRIS data were also used but because of some system problems with the sensor, only small parts of the data were utilized.. AVIRIS was flown on the Twin Otter turboprop at approximately 4000m above the ground with 4m spatial resolution on November 11, 1999 and September 10, 2001. The Hyperion provided 242 spectral bands (from 0.4 to 2.5 µm) with a 30 meter spatial resolution and covered 7.5km by 200km area. An RDACS-3 imagery

with 120 spectral bands and 2x4m spatial resolution was collected at 2350m above the ground by the ITD Spectral Visions. Hyperion was NASA's first hyperspectral imager aboard NASA's Earth Observing-1 (EO-1) spacecraft, which had three land imaging instruments; Advanced Land Imager, Hyperion, and Atmospheric Corrector.

4. METHOD

Hyperspectral imagery can be considered as a single image dataset with a continuous spectrum of radiance (or reflectance) values associated with each image pixel (Bateson and Curtiss, 1996). Hyperspectral imagery can distinguish between slope and brightness variations and resolve absorption bands in the spectrum, which can allow one to identify surface material such as specific minerals or any material with absorption features (Clark *et al.*, 1992). AVIRIS was the first airborne hyperspectral sensor to measure reflected solar radiation from 400nm to 2500 nm (Green *et al.,* 1998).

Individual bands of the RDACS hyperspectral datasets were calibrated to percent reflectance using the known reflectances of two gray scale placards placed on the ground during the overflight (Figure 4). The calibration and radiance to reflectance conversions for the Hyperion dataset were done using several ground targets (dark, medium and light areas), for which ground spectra were collected using the field spectrometer. A simple linear regression model was used in the calibration and conversion process.

Red: Band-86 (1003.37 nm)
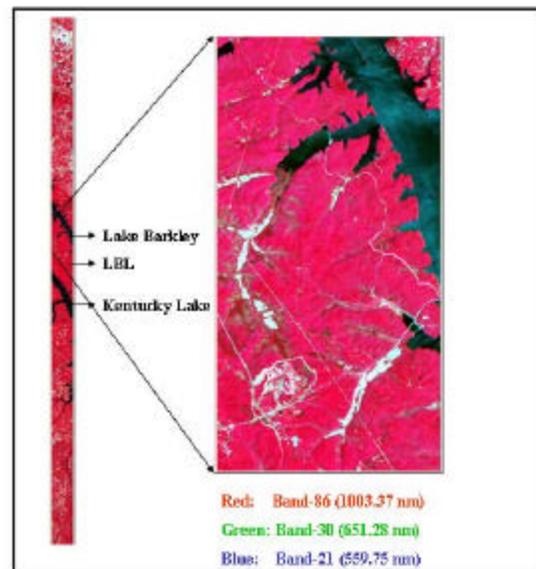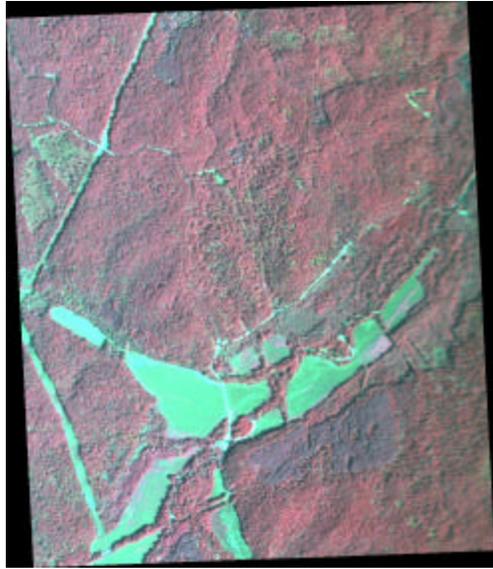Green: Band-30 (651.28 nm)
Blue: Band-21 (559.75 nm)

Figure 2. The Hyperion dataset, April 29, 2001

A spectral library of surface material (endmembers) and vegetation species (Table 1 and Figure 5) was created for hyperspectral analysis of the datasets. Several techniques

Figure 3. The RDACS dataset , September 7, 1999

including the Pixel Purity Index (PPI), an n-Dimensional Visualizer, Spectral Angle Mapper (SAM) and Binary Encoding were utilized to map the study datasets.

For detailed classification, the n-Dimensional Probability Functions (nPDF) approach was used (Cetin, 1990; Cetin and Levandowski, 1991; Cetin *et al.,* 1993). The nPDF techniques is an interactive
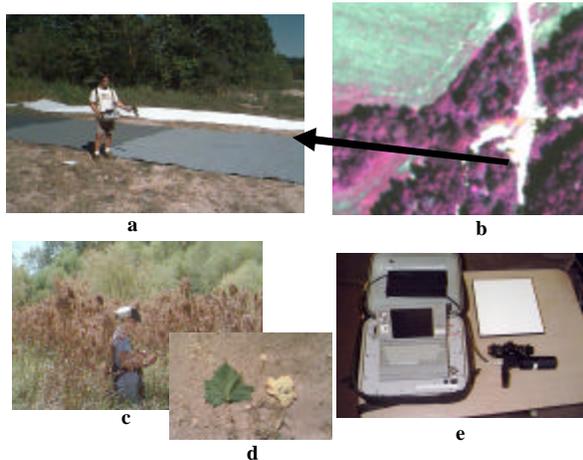

Figure 4. a) Gray-scale placards, b) RDACS imafe showing the location of the placards, c) GPS measurement, d) sycamore leaves; healthy and under stress, and e) Full range (350-2500nm) field spectroradiometer used in this study

image analysis technique, which overcomes many of the inherent limitations of traditional classifiers. The techniques has applications in three broad areas: data visualization, enhancement and classification. For data visualization, nPDF
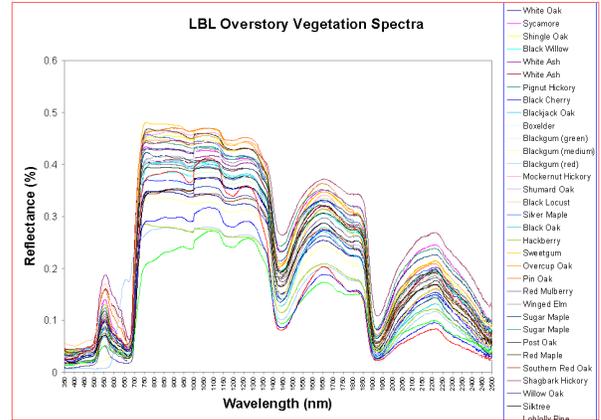

Figure 5. Spectra of the vegetation species in LBL

provides a method for transforming multiple bands of data in a predictable, and scene-independent way. These transformations may be designed so as to enhance a particular cover-type, or to give the best visual representation of the multi-band image data. Spectral frequency plots of the nPDF components give a spectral view of data distribution that can be used to investigate the number and distribution of spectral classes in a high dimensional data set. In addition, these plots are used in a non-parametric classification of the image for discrimination of discrete classes, as well as for classes that are mixtures at the sub-pixel scale. In a mixed deciduous and coniferous forest an nPDF Deciduous Forest Index showed a high correlation with percent deciduous vegetation determined from field surveys.

The nPDF approach may be explained using a cube model. A generalized distribution of highly correlated digital remotely sensed data in three dimensional feature space is shown in Figure 1. In three-dimensional feature space the feature vector is defined by X=[x1,x2,x3]. The location of a point within the range of the total possible measurement space can be described by the distances to the two corners of the cube shown in Figure 6. They are:

$$D_1 = (x_1^2 + x_2^2 + x_3^2)^{1/2}, \tag{1}$$

$$D_2 = [x_1^2 + x_2^2 + (R - x_3)^2]^{1/2} \tag{2}$$

For the multi-dimensional case, the feature vector is defined by X=[x1,x2,x3,...,x_n], where n is the dimension of the data and R is the maximum possible range of the data (255 for 8 bit data.) When a hyper-dimensional cube is used, the vector magnitudes (the distances to the two corners) for n-dimensional data are:

$$D_1 = \left(\sum_{j=1}^{n} x_j^2 \right)^{1/2} \tag{3}$$

$$D_2 = \left(\sum_{j=1}^{n} x_j^2 * (1 - a_j) + (R - x_j)^2 * a_j \right)^{1/2} \qquad (4)$$

where j is the band number. A generalized formula for the distance to the corners of a hyper-dimensional cube can be written as (i is the corner or component number):

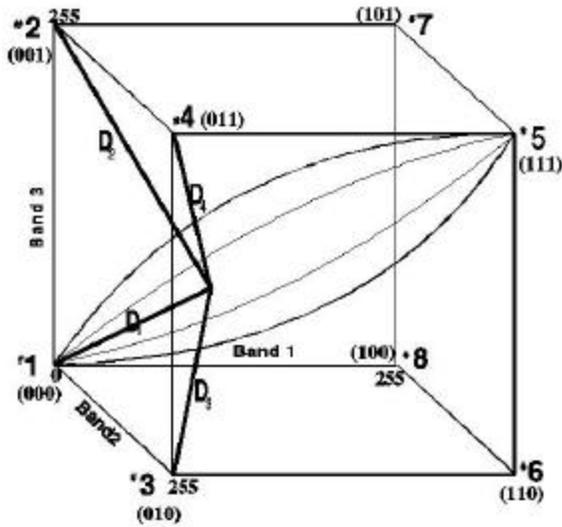$$D_i = \left(\sum_{j=1}^{n} x_j^2 * (1 - a_j) + (R - x_j)^2 * a_j \right)^{1/2} \qquad (5)$$

Figure 6. nPDF Cube Model

There are eight possible corners of a three-dimensional cube as is shown in Figure 6. Four of the corners can be selected as principal corners (1 through 4), the remaining corners (5 through 8) are the complimentary to the four principal corners. For the hyper-dimensional cube model, "a" values for the equation (5) are as follows (j is the band number):

D_1 : For all j values $\qquad$ a = 0

D_2 : if $\begin{cases} j = 1,2,4,5,\ldots & a = 0 \\ j = 3,6,\ldots & a = 1 \end{cases}$

D_3 : if $\begin{cases} j = 1,3,4,6,\ldots & a = 0 \\ j = 2,5,\ldots & a = 1 \end{cases}$

D_4 : if $\begin{cases} j = 1,4,\ldots & a = 0 \\ j = 2,3,5,6,\ldots & a = 1 \end{cases}$

The nPDF formula is:

$$nPDF_i = S * D_i / (2^{BIT} * NB^{1/2}) \qquad (6)$$

where:

$nPDF_i$ $\quad$ = Component i of nPDF,
$\quad i$ $\quad$ = Corner number,
$\quad S$ $\quad$ = Desired scale for the nPDF axes,
$\quad D_i$ $\quad$ = Calculated distance for component i,
$\quad BIT$ = Number of bits of input data,
$\quad NB$ = Number of bands used.

Frequency plots of two nPDF components (hyper-dimensional distances) provide an excellent perspective of multidimensional data distribution. Depending on the spectral distribution of the classes of interest, the user can select corners which provide the maximum separation of the classes. A convenient scale for these nPDF components is 8 bit in range, and thus a two-dimensional frequency plot requires a 256 by 256 array.

The cube model has the advantage of being a conceptually simple way of describing corners in multidimensional space. However, it does tend to limit the choice of corners for four and higher dimensional data. Where this is a problem, the "a" values (see equation 1) are used to describe the corner location. Thus in Figure 6, corner #2 is also labeled (001), which can be interpreted as a corner that has "a" value of zero for the first two bands, and that of one in the third band. Using this convention, the length of the list of "a" values depends on the number of input bands, and thus the corner corresponding to the origin in a four band image would be described as (0000).

Prior to the classification process the spectral values for the entire scene are transformed into nPDF space. The software allows the user to view the distribution of the data and enhance the data by interactively stretching and rotating. This allows a rough visual identification of separable classes. For the supervised classification procedure the training field data are then plotted into nPDF space. Polygons can then be drawn around the obvious classes to delineate the spectral boundaries. The classification procedure uses the boundaries of these polygons to assign pixels to the appropriate class.

5. RESULTS AND DISCUSSION

Classification of the RDACS-3 dataset provided the highest overall accuracy (76% overall accuracy for the overstory species classification and 94% overall accuracy for the other land cover classes such as agriculture fields). The AVIRIS datasets provided an overall accuracy of 69% for the overstory species and 83% for the other land cover classes. The Hyperion dataset provided 62% overall accuracy for the overstory species and 81% for the other classes (Figures 7 and 8; tones of red were used for the forest species).

A comparison between the classifications indicated that they were significantly different. A Z statistic of 3.7 (Hyperion and RDACS-3) and a Z statistic of 4.5 ((Hyperion and AVIRIS) were computed for the pairwise comparisons. Because the Z statistic values were greater than 1.96, there were significant differences in the results of the classifications of the sensors.
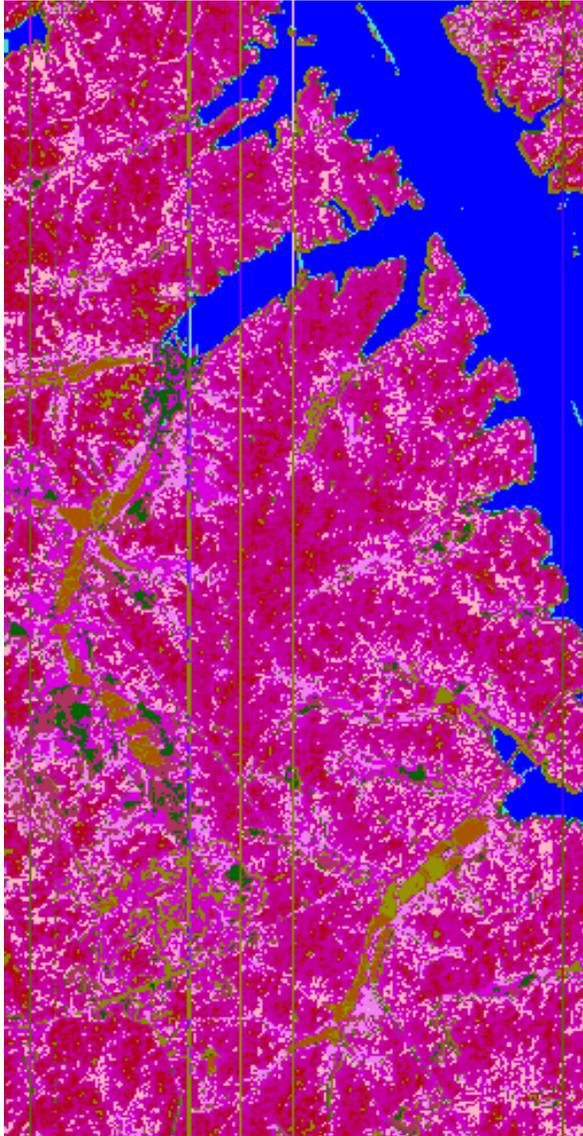

Figure 7. Classification map of the Hyperion dataset

Another objective of this research was to outline forested areas that were under stress due to a drought. Figure 9 shows the spectra of black willow leaves; healthy (cyan, green and red lines), moderately stressed (blue) and severely stressed (black). Another objective was to map the water quality in the lakes using the hyperspectral data (Figure 10). However, because of the page limitations, these studies were not included in this paper.
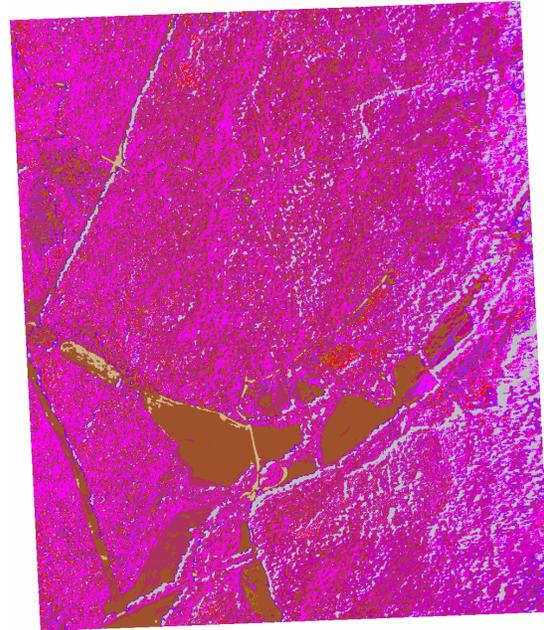

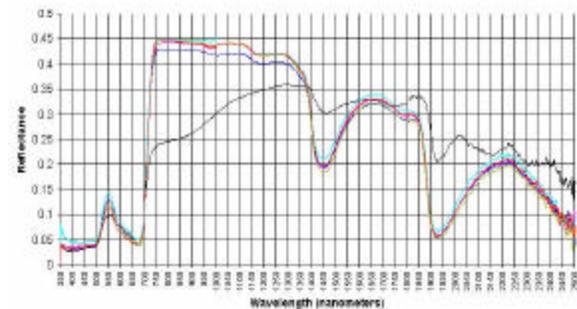Figure 8. Classification map of the RDACS-3 dataset

Figure 9. Spectra of black willow; healthy and under stress (the scale is between 0 and 1 (100%) for the reflectance axis)

6. CONCLUSIONS

Airborne and spaceborne hyperspectral imagery is becoming increasingly accessible due to the increasing number of companies and agencies operating hyperspectral scanners. Airborne data acquisitions benefit greatly over satellite based missions because the user has influence on the mission in terms of time schedules, flight line arrangements, calibration measurements, spectral/spatial resolutions, and acceptable weather conditions. However, airborne hyperspectral sensors are often very expensive due to fact that limited spatial coverage and multiple flight lines may be required to cover a study area. Also, data processing is usually complex and can cause problems.

Airborne hyperspectral sensors are usually used to test spaceborne hyperspectral sensors, which provide continuous coverage of most of our planet as well planetary surfaces .
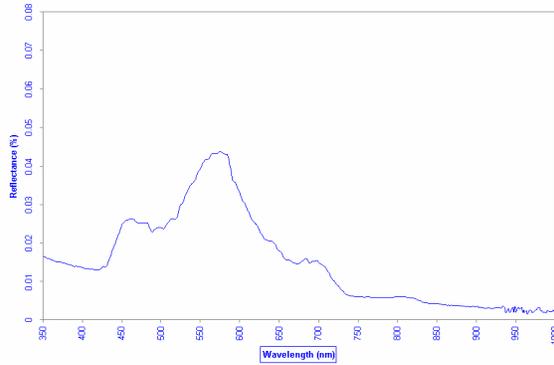
Figure 10. High resolution spectra of Kentucky Lake (the scale is between 0 and 1 (100%) for the reflectance axis)

The RDACS data used in this study provided the highest accuracy in terms of classification of individual overstory species. Although AVIRIS generally provides very good results, the datasets collected for the study area had many problems. Only very limited areas could be used to classify the land cover; therefore, the AVIRIS datasets were not fully utilized in the comparison process. Although the Hyperion data had a low spatial resolution, the results showed that the data could be used for mapping of vegetation alliances in forestry related studies. Water quality studies using the Hyperion sensor should be more cost effective than using airborne hyperspectral imagery.

7. REFERENCES

Adams, J. B., M. O. Smith, and P. E. Johnson, 1986. Spectral mixture modeling: A new analysis of rock and soil types at Viking Lander 1 site. *Journal of Geophysical Research (JGR),* 91:8098-8112.

Bateson, A., and B. Curtiss, 1996. A method for manual endmember selection and spectral unmixing. *Remote Sensing of the Environment*, 55:229-243.

Boardman, J. W., 1990. Inversion of high spectral resolution data. *Society of Photo-Optical Instrumentation Engineers (SPIE),* 1298:222-233.

Cetin, H., 1990. nPDF-An algorithm for mapping n-dimensional probability density functions for remotely sensed data. *Proceedings of the 10th Annual International Geoscience & Remote Sensing Symposium, IGARSS'90*, I: 353-356.

Cetin, H. and Levandowski, D. W., 1991. Interactive classification and mapping of multi-dimensional remotely sensed data using n-dimensional probability density functions (nPDF). *Photogrammetric Engineering and Remote Sensing*, 57(12): 1579-1587.

Cetin, H., Warner, T. A., and Levandowski, D. W., 1993. Data classification, visualization and enhancement using n-dimensional probability density functions (nPDF): AVIRIS, TIMS, TM and geophysical applications. *Photogrammetric Engineering and Remote Sensing,* 59(12): 1755-1764.

Clark, R.N, G.A. Swayze, and A. Gallagher, 1992. Mapping the mineralogy and lithology of canyonlands, Utah with imaging spectrometer data and the Multiple Spectral Feature Mapping Algorithm. *The Third Annual JPL Airborne Geosciences Workshop, Volume I: AVIRIS Workshop; JPL Publication*, 92-14:11-13

Cloutis, E. A., 1996. Hyperspectral geological remote sensing: evaluation of analytical techniques. *International Journal of Remote Sensing*, 17(12):2215-2242.

Dwyer, J. L., F. A. Kruse, and A. B. Lefkoff, 1995, Effects of empirical versus model-based reflectance calibration on automated analysis of imaging spectrometer data: A case study from the Drum Mountains, Utah. *Photogrammetric Engineering and Remote Sensing,* 61:1247-1254.

Green, R.O., M.L. Eastwood, C.M. Sarture, T.G. Chrien, M. Aronsson, B.J. Chippendale, J.A. Faust, B.E. Pauri, C.J. Chovit, M. Solis, M.R. Olah and O. Williams, 1998. Imaging Spectroscopy and the Airborne Visible/Infrared Imaging Spectrometer (AVIRIS). *Remote Sensing of the Environment*, 65:227-248.

Huete, A., Justice, C., and Liu, H., 1994. Development of vegetation and oil indices for MODIS-EOS. *Remote Sensing of Environment*, 49:224-234.

Jakubauskas, M.E., and Price, K.E., 1997. Empirical relationships between structural and spectral factors of Yellowstone Lodgepole pine forests. *Photogrammetric Engineering and Remote Sensing*, 63(12):1375-1381.

Lee, C. and D. A. Landgrebe, 1993. Analyzing high-dimensional multispectral data. *IEEE Transactions on Geoscience and Remote Sensing,* 31 (4):792-800.

Marmo, J., 1996. Hyperspectral imager will view many colors of earth. *Laser FocusWorld*, 8:85-92.

Martin, M. E. and J. D. Aber, 1997. High spectral resolution remote sensing of forest canopy lignin, nitrogen, and ecosystem processes. *Ecological Applications,* 7 (2):431-443.

Mustard, J. F., and Pieters, 1987. Quantitative abundance estimates from bidirection reflectance measurements. *The 17th Lunar Planet Science Conference, JGR, supplemen,:* 92:E617-E626.

8. ACKNOWLEDGMENTS